B.Bilgic1,V.K.Goyal1,andE.Adalsteinsson1,2
1EECS,MIT,Cambridge,MA,UnitedStates, 2Harvard-MITDivisionofHealthSciencesandTechnology,MIT,Cambridge,MA,UnitedStates

INTRODUCTION: Clinical MRI routinely relies on multiple acquisitions of the same region of interest with several different contrasts. We present a reconstruction algorithm based on Bayesian compressed sensing to exploit such multi-contrast acquisitions for accelerated imaging by jointly reconstructing a set of related images from undersampled *k*-space. Our method offers better performance than when the images are either reconstructed individually [1], or jointly by a previously proposed method, M-FOCUSS [2].

THEORY: Let the signals $\{\boldsymbol{x}_i\}_{i=1}^{L} \in \mathbb{R}^M$ represent MRI scans with different image weightings. We obtain a sparse representation by modifying the undersampled *k*-space data $\boldsymbol{y}_i$ according to $\mathbf{F}_i\boldsymbol{\delta}_i^x = (1-e^{-2\pi j\omega/n})\boldsymbol{y}_i \equiv \boldsymbol{y}_i^x$, where $\mathbf{F}_i \in \mathbb{C}^{K_i \times M}$ are undersampled Fourier operators, $\boldsymbol{\delta}_i^x$ is the i^{th} vertical image gradient, $\boldsymbol{y}_i^x$ are modified observations, ω is the vertical frequency index; and we have an analogous equations for horizontal gradients $\boldsymbol{\delta}_i^y$. We model the data as being corrupted by Gaussian noise with variance σ^2 via $\boldsymbol{y}_i^x = \mathbf{F}_i\boldsymbol{\delta}_i^x + \boldsymbol{n}_i$. To take the complex nature of noise into account, we modify the observations as $[\mathcal{R}(\boldsymbol{y}_i^x);\mathcal{I}(\boldsymbol{y}_i^x)] = [\mathcal{R}(\mathbf{F}_i);\mathcal{I}(\mathbf{F}_i)]\boldsymbol{\delta}_i^x + [\mathcal{R}(\boldsymbol{n}_i);\mathcal{I}(\boldsymbol{n}_i)]$, which we concisely rewrite as $\boldsymbol{Y}_i^x = \boldsymbol{\Phi}_i\boldsymbol{\delta}_i^x + \boldsymbol{N}_i$, where $\mathcal{R}(.)$ and $\mathcal{I}(.)$ indicate real and imaginary parts. We model the sparse coefficients to be drawn from a product of Normal distributions with variances determined by the hyperparameters $\boldsymbol{\alpha} = \{\alpha_j\}_{j=1}^{M}$ and the noise precision parameter $\alpha_0 = \sigma^{-2}$ as, $p(\boldsymbol{\delta}_i^x|\boldsymbol{\alpha},\alpha_0) = \prod_{j=1}^{M}\mathcal{N}(\delta_{i,j}{}^x|0,\alpha_j^{-1}\alpha_0^{-1})$ where $\mathcal{N}(\cdot|0,\alpha_j^{-1}\alpha_0^{-1})$ is a zero-mean Gaussian with variance $\alpha_j^{-1}\alpha_0^{-1}$. We also define a Gamma prior over α_0, so that the posterior $p(\boldsymbol{\delta}_i^x|\boldsymbol{Y}_i^x,\boldsymbol{\alpha})$ can be analytically computed to yield a Student-*t* distribution having mean $\boldsymbol{\mu}_i = \boldsymbol{\Sigma}_i\boldsymbol{\Phi}_i{}^T\boldsymbol{Y}_i^x$ and covariance $\boldsymbol{\Sigma}_i = (\boldsymbol{\Phi}_i{}^T\boldsymbol{\Phi}_i + \mathbf{A})^{-1}$ with $\mathbf{A} = diag(\alpha_1,\ldots,\alpha_M)$. To evaluate this posterior, we estimate $\boldsymbol{\alpha}$ via maximum likelihood by maximizing $\mathcal{L}(\boldsymbol{\alpha}) = \sum_{i=1}^{L} p(\boldsymbol{Y}_i^x|\boldsymbol{\alpha})$ [3]. Once the gradients $\{\boldsymbol{\delta}_i^x\}_{i=1}^{L}$ and $\{\boldsymbol{\delta}_i^y\}_{i=1}^{L}$ are obtained, we find images $\{\boldsymbol{x}_i\}_{i=1}^{L}$ that are consistent with these and *k*-space measurements $\{\boldsymbol{y}_i\}_{i=1}^{L}$ by solving a least squares problem.

METHODS: To demonstrate the performance of Bayesian CS, two datasets were reconstructed. The first set consists of T2-weighted images obtained with two different TE's using a TSE sequence (256×256 pixels, 1×1×3 mm^3, TR=6000, TE_1=27, TE_2=94 ms). A single slice was retrospectively undersampled along phase encoding with acceleration R = 2.5 using a different mask for each image. The SRI24 atlas [4] features proton density, T2 and T1 weighted scans at 256×256 resolution. A single slice from the atlas was retrospectively undersampled along phase encoding with acceleration R = 4 using different undersampling masks. Both datasets were reconstructed using the algorithm in [1], M-FOCUSS joint reconstruction method [2] and joint Bayesian CS.

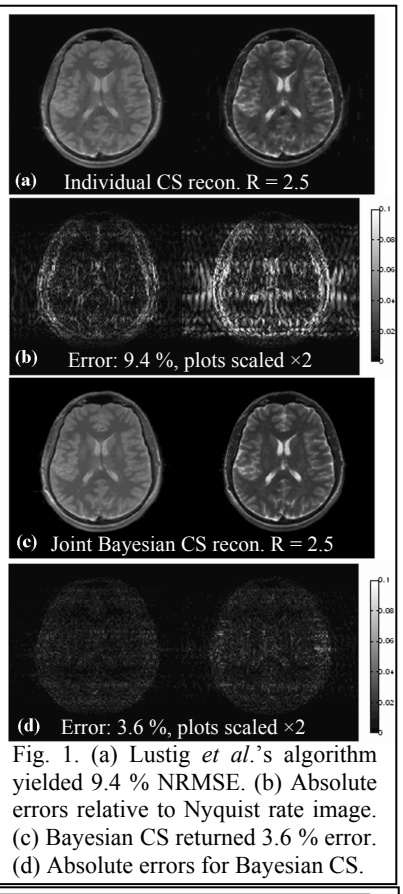

Fig. 1. (a) Lustig *et al*.'s algorithm yielded 9.4 % NRMSE. (b) Absolute errors relative to Nyquist rate image. (c) Bayesian CS returned 3.6 % error. (d) Absolute errors for Bayesian CS.

RESULTS: Fig. 1 depicts reconstruction results for the TSE dataset. Here, Lustig *et al*.'s algorithm [1] returned 9.4% NRMSE (normalized root-mean-square error), while the error was 5.1% and 3.6% for M-FOCUSS (not depicted) and joint Bayesian method, respectively. The reconstructions took 26 minutes for [1], 4 minutes for [2] and 29.9 *hours* for Bayesian CS. SRI24 atlas reconstruction results are given in Fig. 2, wherein Lustig *et al*.'s code yielded 9.4% NRMSE, while M-FOCUSS (not depicted) and joint Bayesian CS had 3.2% and 2.3% error, respectively. The reconstruction times were 43 minutes for [1], 5 minutes for [2] and 26.4 *hours* for Bayesian CS.

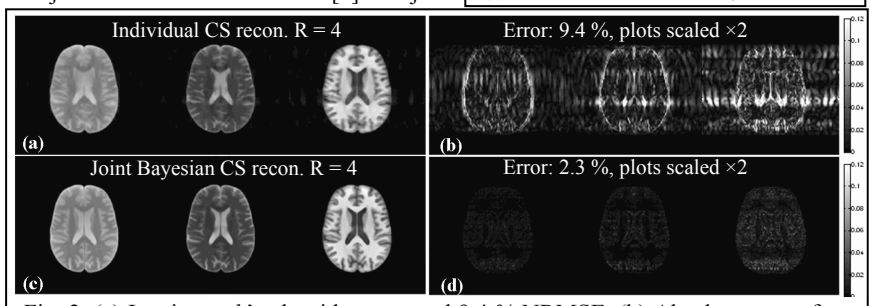

Fig. 2. (a) Lustig *et al*.'s algorithm returned 9.4 % NRMSE. (b) Absolute errors for gradient descent. (c) Bayesian CS yielded 2.3 % error. (d) Errors for Bayesian CS.

DISCUSSION: The success of the joint Bayesian CS algorithm is based on the premise that the multi-contrast scans share a set of similar gradients. While estimating $\boldsymbol{\alpha}$, data from all L scans contribute to likelihood maximization procedure and once the point estimates are constituted, the posterior for the signal coefficients $\boldsymbol{\delta}_i^x$ is estimated based only on its related *k*-space data $\boldsymbol{Y}_i^x$ due to $\boldsymbol{\mu}_i = \boldsymbol{\Sigma}_i\boldsymbol{\Phi}_i{}^T\boldsymbol{Y}_i^x$. This formulation renders Bayesian CS flexible enough to support idiosyncratic image features, while still enabling information sharing among images. Currently, the long reconstruction times of the Bayesian algorithm make it prohibitive for clinical use as implemented, but we expect future implementations on graphics processing units to overcome this drawback and enable the application of joint image reconstructions to highly-accelerated image acquisitions. This joint reconstruction paradigm extends to other MR applications where priors occur naturally and sparsity features are shared including, e.g., spectroscopic imaging joint with structural MRI, and quantitative susceptibility mapping joint with the magnitude of structural MRI.

REFERENCES: [1] Lustig M *et al*. MRM 2007; 58(6):1182-1195. [2] Cotter SF *et al*. IEEE T Signal Proces 2005; 53(7):2477-2488. [3] Ji SH *et al*. IEEE T Signal Proces 2009; 57(1):92-106. [4] Rohlfing T *et al*. Hum Brain Mapp 2010; 31(5):798-819.